Journal of Geoscience and Environment Protection, 2023, 11, 64-89
https://www.scirp.org/journal/gep
ISSN Online: 2327-4344
ISSN Print: 2327-4336

Structural Mapping of Kakobola and Its Surroundings by Analyzing Geomagnetic Data

Jonathan Musitu Muliwavyo[1,2], Albert Mbata Muliwavyo[3], Lumière Musitu[3], Jean-Marie Tshitenge Mbuebue[3], Clément N'Zau Umba-Di-Mbudi[1,2,4]

[1]Mention Geosciences, Faculty of Sciences and Technologies, University of Kinshasa, Kinshasa, Democratic Republic of the Congo
[2]Geo-Hydro-Energy Research Group, Faculty of Science and Technology, University of Kinshasa, Kinshasa, Democratic Republic of the Congo
[3]Mention Physics, Faculty of Science and Technology, University of Kinshasa, Kinshasa, Democratic Republic of the Congo
[4]Faculty of Polytechnic, President Joseph Kasa-Vubu State University, Boma, Democratic Republic of the Congo
Email: musitujosephjo@gmail.com, albert.mbata@unikin.ac.cd, mbaalbert@gmail.com, lumieremusitu4@gmail.com, jeanmarie.tshitenge@unikin.ac.cd, Clement.mbudi@unikin.ac.cd

How to cite this paper: Musitu Muliwavyo, J., Mbata Muliwavyo, A., Musitu, L., Tshitenge Mbuebue, J.-M., & Umba-Di-Mbudi, C. N. (2023). Structural Mapping of Kakobola and Its Surroundings by Analyzing Geomagnetic Data. *Journal of Geoscience and Environment Protection, 11,* 64-89.
https://doi.org/10.4236/gep.2023.119006

Received: July 26, 2023
Accepted: September 11, 2023
Published: September 14, 2023

Abstract

This study focuses on the Kakobola region and its surroundings where cavities discovered in its basement may represent a major risk for the hydroelectric dam erected on the Lufuku River near the Kakobola city and the civil engineering works in the study area. In order to deepen the studies related to this understudied region and provide decision-makers with information that will enable them to make the necessary and appropriate decisions regarding the development of this area, a study based on the analysis of geomagnetic data was carried out using certain methods revealing more shallow than deep structures, and others highlighting the limits of both shallower and deeper structures. Total magnetic anomalies and reduced to equator (RTE) magnetic anomalies were used to map the subsurface of the Kakobola region and its surroundings. In order to detect the edges of magnetized structures, the horizontal gradient magnitude (HGM), the analytic signal (AS), the horizontal gradient of tilt angle (HGTA), the tilt angle (TA), the theta map (TM), the enhanced total horizontal derivative of the tilt angle (ETHDR), the tilt angle of the horizontal gradient (TAHG), and the tilt angle of analytic signal (TAAS) were used. The study area is characterized by two areas of low values of magnetic anomalies and two other sources of high magnetic anomalies located in the bed and the neighborhood of the two major rivers in the region. The shallow sources of magnetic anomalies are lying in the bed and the vicinity of the same rivers in the study area. The magnetic sources in the study area are connected and almost linear. Several magnetic lineaments identified in this region by different methods present several preferential directions, but the most predominant directions are NE-SW, NW-SE, W-E and NE-SW.

Keywords

Magnetic Anomalies, HGM, TAHG, Lineaments, Shallow Structures

1. Introduction

This study focuses on the Kakobola region and its surroundings, an understudied region that has attracts the attention of certain researchers since the erection of a hydroelectric dam on the Lufuku River near the Kakobola city (Ndala et al., 2022, 2023). Cavities have been detected in the subsoil of the study area (Tshiwisa et al., 2023). These cavities represent a major risk for this dam and the civil engineering works that may be undertaken in this region. In order to enhance the understanding of the subsoil characteristics and provide decision-makers with information that will enable them to make the appropriate decisions regarding the development of this area, a study based on the analysis of geomagnetic data can be carried out using certain methods revealing more shallow than deep structures, and others highlighting the limits of deep and deeper structures. Some of these methods can be applied to total magnetic anomalies without reduction to the equator while other methods, before their application, require reduced to equator magnetic anomalies for our study region. These delineating methods are ubiquitous in edge detection.

Edge detection is essential in enhancing and interpreting the geologic features of potential field data (Prasad et al., 2022). Locating the horizontal boundaries of magnetic and gravity sources (Pham, 2020) is an essential task in characterizing a geological site. In a dataset, adjacent anomalous sources due to their field superposition cannot be differentiated. In particular, when shallow and deep magnetic or gravity anomaly sources overlap, delineating the edges of these strong and weak amplitude anomaly sources is a difficult task (Nasuti & Nasuti, 2018; Nasuti et al., 2018). In order to identify the horizontal extents of subsurface structures and distinctly display the edges of anomaly sources of different depths, various edge detection methods have been proposed (Prasad et al., 2022; Pham et al., 2021a). Most of the edge enhancement techniques depend either on the horizontal gradient or on the total gradient of the potential fields. These filters are generally constructed based on vertical and horizontal gradients of the magnetic and gravity data (Pham, 2020). Each edge detection filter has as well as its own advantages and shortcomings, depending on the nature of the potential field data (Prasad et al., 2022). Therefore, the use of different edge detection filters can be recommended in order to ascertain lateral limits of magnetic anomaly sources as Ghil et al. (2002) recommend in climatology.

HGM and AS filters in potential field data interpretation are more effective in displaying the edges of shallower sources than those of deeper ones because these filters are dominated by high-amplitude anomalies (Arisoy & Dikmen, 2013).

Therefore, they cannot balance the anomalies' amplitudes due to the geological structures located at different depths (Pham et al., 2022). In order to balance smaller and larger amplitudes of potential field anomalies by normalizing derivatives of the field (Ferreira et al., 2013), numerous balanced or normalized derivative methods have been designed (Arisoy & Dikmen, 2013; Eldosouky et al., 2020; Prasad et al., 2022). However, all normalized derivative methods delineate the anomaly sources of different depths, but present a diffuse response to deeper structures.

Many researchers propose enhanced edge detector methods that should produce very clear resolution at a time in shallow subsurface structures and in deeper structures. These edge detectors should outline the edges of geological structures very well in the presence of many anomaly sources and when some of the anomaly sources are very close to each other (Arisoy & Dikmen, 2013). Precise delineation of the horizontal positions of the anomaly sources is one of the requirements for each edge detector filter (Pham et al., 2022). Thus, the choice and the use of numerous edge detection filters in delineating geological bodies are of extreme importance. Miller and Singh (1994) first developed the TA, and Verduzco et al. (2004) presented an alternative method as the total horizontal derivative of TA. The tilt derivative method can be used for estimating the basement depths (Salem et al., 2007).

The horizontal edges and boundaries of magnetic bodies often indicate subsurface lithological contacts, fractures, and different tectonic characteristics, which are helpful for interpreting geological features (Eldosouky et al., 2020). According to Domzalski (1966), the analysis of magnetic anomalies can be used to map lineaments, deep contacts, depth of sediment cover and mineralization.

The subsoil magnetic mapping of the study area is the subject of our concerns. The objectives of this work are to delineate magnetic bodies, highlight the presence of fractures and/or lithological contacts hidden by the Kalahari sand in our study area, and determine the preferential directions of the lithological contacts and/or faults present in the region as well as their dips.

To achieve these goals, we have opted for the use of different methods based on different concepts and/or different hypotheses as recommended by Ghil et al. (2002). The different methods that will be applied to the magnetic data of our study area are:

- The upward continuation and the reduction to the equator as data processing methods, the first one can reveal shallow sources of magnetic anomalies and deep sources of magnetic anomalies;
- The standard deviation (SD) as a dispersion indicator of magnetic anomaly sources in the study area;
- The analytic signal (AS), the horizontal gradient magnitude (HGM) and the horizontal gradient of tilt angle (HGTA) for delineating shallow magnetic anomaly sources;
- The theta map (TM), the tilt angle (TA), the tilt angle of horizontal gradient (TAHG), the tilt angle of analytic signal (TAAS), and the enhanced total ho-

rizontal derivative of the tilt angle (ETHDR) for delineating shallow and deep magnetic anomaly sources.

The AS and the TAAS do not require reduction to a pole or the equator.

2. Geologic Setting of the Study Area

The study area is located in the southeast of Kwilu province in the Democratic Republic of the Congo (DRC) on latitude 05˚30'S to 06˚00'S and longitude 19˚00'E to 19˚30'E (**Figure 1**).

The Kalahari sand being too thick covers the geological structures present in the region. Geologically, our area is made up of sedimentary formations. These sedimentary formations include from bottom to top the Kwango series followed by the Kalahari system comprising two series presenting as follows from bottom to top (De Ploey et al., 1968): the upper series of ocher sands dating from the Neogene and the lower series of polymorphic sandstones attributed to the Paleogene (**Figure 2**).

3. Data and Methods

3.1. Materials and Data Processing

Earth magnetic field data for Kakobola and its surroundings were obtained on 12/18/2019 through the World Magnetic Model (WMM) software. These data relate to the region between longitudes 18.6˚E and 19.6˚E, latitudes 5.20˚S and 6.50˚S and at an altitude of 300 m above the topography. These data recorded individually in Excel come from 1479 virtual mesh stations equidistant from 3.69 km. **Figure 3** shows the Earth's magnetic field data grid created in Oasis montaj 8.4.

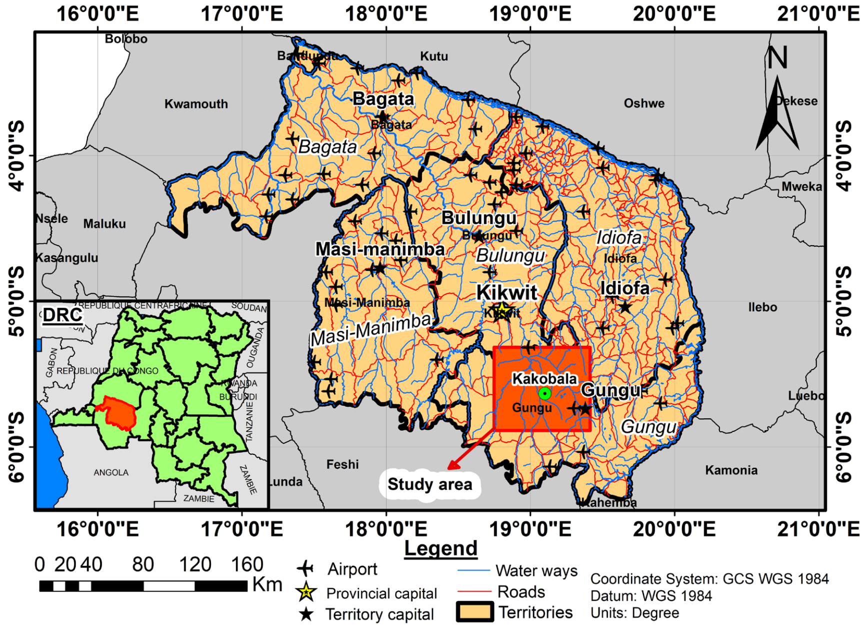

Figure 1. Location of study area.

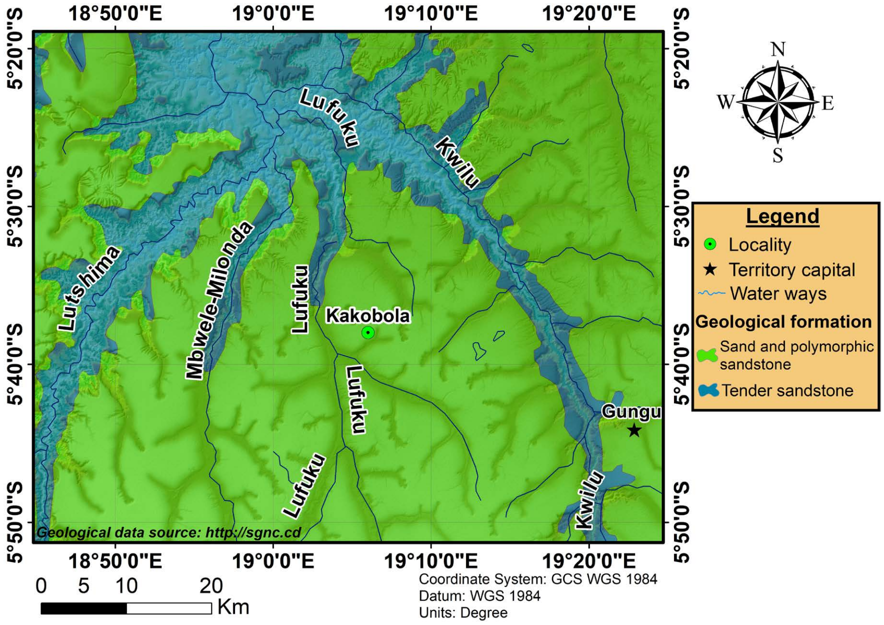

Figure 2. Geological map of our study region.

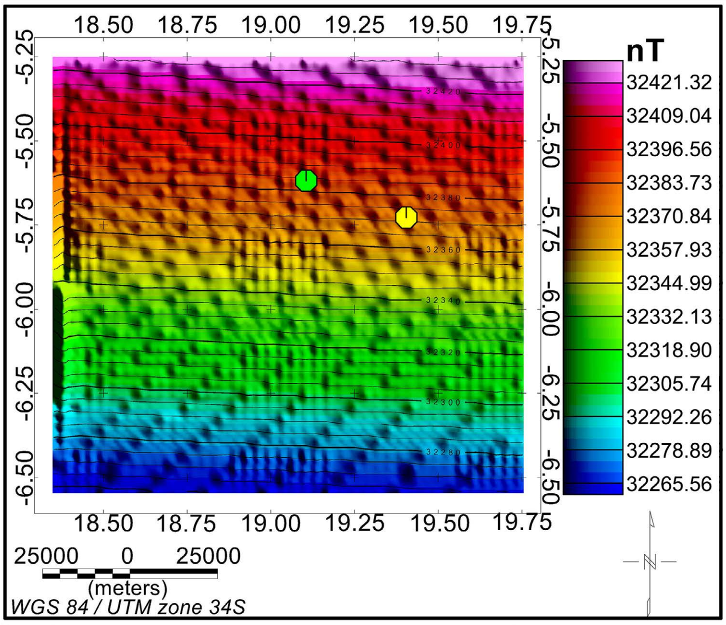

Figure 3. Earth's magnetic field of our study area. Kakobola in green circle and Gungu in yellow circle.

3.1.1. Reduction to the Equator

The reduction to the equator filter allows anomalies to be represented as if they had been measured at the magnetic equator. The reduction at the equator of a total field anomaly is given by the equation (Blakely, 1995).

3.1.2. Upward Continuation Method

The upward continuation is a category of low pass filter used to attenuate high frequencies in order to emphasize regional anomalies (those with long wavelengths). The continuation of the field at an elevation above the reference level is defined by Blakely (1995).

3.1.3. Other Processing Data

The RTE data grid is used to obtain the analytic signal grid using the Oasis montaj software. The analytic signal grid is then used to map the depth of the roof of the sources of the magnetic anomalies resulting from the analytic signal.

The maxima resulting from the tilt angle enable us to map the lineaments resulting from the tilt angle using PCI Geomatica 2016 software. The lineaments resulting from the tilt angle are vectorized in ArcMap, then brought back into Rockworks to make the rose diagram in order to know the preferential directions. The lineament density map is made using vectorized lineaments in ArcMap.

The RTE data grid was filtered in Oasis montaj 8.4 to obtain the FTHDT.

The high-pass filter implemented in the Surfer 21 software allowed us to map the regional anomalies arising from the RTE.

The lineaments were vectorized through ArcMap to map the lineaments of the DS The vectorized lineaments were used to make the lineament density map in ArcMap and the rose diagram in Rockworks. The vectorized lineaments in ArcMap were used to make the lineament density map and to make the rose diagram.

The maxima resulting from the tilt angle enabled us to map the lineaments resulting from the tilt angle using PCI Geomatica software. The lineaments resulting from the tilt angle were vectorized in ArcMap then brought back into Rockworks to make the Rose diagram in order to know the preferential directions. The lineament density map was made using vectorized lineaments in ArcMap.

3.2. Methods of Study

Amplitude-based filters used to extract the boundaries of the anomaly sources are effective only to determine the edges of high amplitude anomaly sources that are in fact shallow sources (Arisoy & Dikmen, 2013; Pham, 2020). Among the most used filters of this category, we cite the horizontal gradient magnitude (HGM) denoted also total horizontal derivative (THDR) and the analytic signal (AS) called also total gradient (TG). In order to determine edges of both weak and strong amplitude anomaly sources, numerous phase-based filters developed use normalized derivatives based on HGM and AS (Pham, 2020).

3.2.1. The Standard Deviation (SD) Method

The standard deviation is used to delineate the local variations of the data. At each grid location, it measures the standard deviation of the data values in the local neighborhood (Elkhateeb et al., 2018). Important features often show a large variation in the background signal. For a window containing N cells whose average value is μ, the standard deviation σ of the cell values is given by:

$$\sigma = \sqrt{\frac{1}{N}\sum_{i=1}^{N}(x_i - \mu)^2} \tag{1}$$

When interpreting the results, values near zero indicate very little variation, while high values indicate large variation.

3.2.2. The Horizontal Gradient Magnitude (HGM)

According to Souga et al. (2020), horizontal gradient magnitude (HGM), called also total horizontal derivative (THDR), is an often-used filter for potential field data. HGM is defined by Cordell and Grauch (1982) as:

$$\mathrm{HGM}(x, y) = \sqrt{\left(\frac{\partial(\Delta F(x, y))}{\partial x}\right)^2 + \left(\frac{\partial(\Delta F(x, y))}{\partial y}\right)^2} \tag{2}$$

where ΔF is the gravity anomaly or total magnetic anomaly. The HGM emphasizes more the edges, the fractures and/or lithologic contacts of the shallow bodies than those of deeper sources (Arisoy & Dikmen, 2013). In HGM results, high amplitude responses from the shallow sources dominate low amplitude responses from deep sources (Pham et al., 2021b). In fact, the HGM filter uses the amplitudes of the derivatives of potential field data (Pham et al., 2021b).

3.2.3. The Analytic Signal (AS) Method

For a magnetic potential field source, the analytic signal (AS) is defined by the equation (Keating & Sailhac, 2004):

$$\mathrm{AS} = \sqrt{\left(\frac{\partial(\Delta B)}{\partial x}\right)^2 + \left(\frac{\partial(\Delta B)}{\partial y}\right)^2 + \left(\frac{\partial(\Delta B)}{\partial z}\right)^2} \tag{3}$$

where ΔB is the total magnetic anomaly. It is based on the use of horizontal and vertical gradients of the potential field (Nabighian, 1972; Roest et al., 1992). In presence of more than one magnetic anomaly source, AS results are dominated by shallow sources. AS maxima of the magnetic data can delineate clearly the edges of the shallower anomaly sources, but are inefficient in delineating the deeper anomaly sources (Arisoy & Dikmen, 2013) because this method use the amplitudes of the derivatives of potential field data (Pham et al., 2021a).

3.2.4. The Tilt Angle (TA) Method

As the first phase-based filter and developed by Miller and Singh (1994), the tilt derivative (TDR), also called tilt angle (TA), is the vertical gradient normalized by the horizontal derivative magnitude (Pham et al., 2021a). It is defined by the equation:

$$\mathrm{TA} = \tan^{-1}\frac{\frac{\partial \Delta F}{\partial z}}{\sqrt{\left(\frac{\partial \Delta F}{\partial x}\right)^2 + \left(\frac{\partial \Delta F}{\partial y}\right)^2}} \tag{4}$$

where ΔF is the gravity anomaly or total magnetic anomaly. The tilt angle amplitude values are restricted to vary only between $-\pi/2$ and $+\pi/2$. Positive over the magnetic sources and negative outside the sources, the amplitude of the tilt angle crosses through zero at or near the edges of the source (Arisoy & Dikmen, 2013).

3.2.5. The Horizontal Gradient of Tilt Angle

Called also total horizontal derivative of tilt angle, the horizontal gradient of tilt angle (HGTA) is defined as (Verduzco et al., 2004):

$$\mathrm{HGTA} = \sqrt{\left(\frac{\partial(\mathrm{TA})}{\partial x}\right)^2 + \left(\frac{\partial(\mathrm{TA})}{\partial y}\right)^2} \tag{5}$$

The HGTA generates maximum values over the edges of the magnetized bodies (Arisoy & Dikmen, 2013; Prasad et al., 2022) and produces secondary edges around the true edge (Prasad et al., 2022), delineates model edges well as the amplitude of the HGTA peaks over magnetic sources (Arisoy & Dikmen, 2013). It has a poor resolution in detecting the boundaries of deeper bodies (Pham, 2020) and strongly amplifies noise in the data in presence of noise (Arisoy & Dikmen, 2013).

3.2.6. The Theta Map (Wijns et al., 2005)

The theta map (TM) is a filter proposed by Wijns et al. (2005). It is the normalization of the THDR by the AS and is defined as

$$\mathrm{TM} = \cos^{-1}\frac{\mathrm{THDR}}{\mathrm{AS}} \tag{6}$$

The TM filter produces balances between edges located at different source depths (Prasad et al., 2022) but does not produce the expected sharp gradient over the edges (Arisoy & Dikmen, 2013). False borders can appear in the edge maps (Pham et al., 2021b).

3.2.7. Tilt Angle of the Horizontal Gradient

Introduced by Ferreira et al. (2013), the tilt derivative of the horizontal derivative (called also tilt angle of horizontal gradient (TAHG)) is defined as:

$$\mathrm{TAHG} = \tan^{-1}\frac{\frac{\partial \mathrm{HGM}}{\partial z}}{\sqrt{\left(\frac{\partial \mathrm{HGM}}{\partial x}\right)^2 + \left(\frac{\partial \mathrm{HGM}}{\partial y}\right)^2}} \tag{7}$$

where

$$\mathrm{HGM} = \sqrt{\left(\frac{\partial \Delta F}{\partial x}\right)^2 + \left(\frac{\partial \Delta F}{\partial y}\right)^2} \tag{8}$$

The TAHG method can generate a balanced image for the anomaly sources located at different depths (Prasad et al., 2022) and detect all the source edges without any false edges (Pham et al., 2021b).

3.2.8. The Tilt Derivative of the Total Gradient

The tilt derivative of the total gradient, called also tilt angle of analytic signal

(TAAS), introduced by Cooper (2014), is based on dividing the vertical derivative of the total gradient grid by the its horizontal derivative magnitude grid and given by the following equation:

$$\text{TAAS} = \tan^{-1}\frac{\dfrac{\partial \text{AS}}{\partial z}}{\sqrt{\left(\dfrac{\partial \text{AS}}{\partial x}\right)^2+\left(\dfrac{\partial \text{AS}}{\partial y}\right)^2}} \tag{9}$$

where

$$\text{AS} = \sqrt{\left(\frac{\partial \Delta F}{\partial x}\right)^2+\left(\frac{\partial \Delta F}{\partial y}\right)^2+\left(\frac{\partial \Delta F}{\partial z}\right)^2} \tag{10}$$

Delineating the boundaries is related to the maximum values of TAAS but detected edges have low resolution (Prasad et al., 2022). The TAAS filter is effective in delineating all the borders, but its performance does not seem to perform well over bodies with superimposed magnetic source bodies.

3.2.9. The Enhanced Total Horizontal Gradient of the Tilt Angle

The edge detector proposed by Arisoy and Dikmen (2013) and denoted "enhanced total horizontal derivative of the tilt angle-ETHDR" is given by the relation:

$$\text{ETHDR} = \sqrt{\left(\frac{\partial \text{ETilt}}{\partial x}\right)^2+\left(\frac{\partial \text{ETilt}}{\partial y}\right)^2} \tag{11}$$

where ETilt filter, the ratio of the vertical derivative (VDR) to the total horizontal derivative of the AS, is given by the equation:

$$\text{ETilt} = \tan^{-1}\left(k\frac{\dfrac{\partial F}{\partial z}}{\sqrt{\left(\dfrac{\partial \text{AS}}{\partial x}\right)^2+\left(\dfrac{\partial \text{AS}}{\partial y}\right)^2}}\right) \tag{12}$$

with

$$k = \frac{1}{\sqrt{(\Delta x)^2+(\Delta y)^2}} \tag{13}$$

where k is the dimensional correction factor. Δx and Δy are sampling intervals in the x and y directions, respectively. According to Arisoy and Dikmen (2013), the ETHDR filter performs better than preceding edge filters in delineating the borders of shallow and deep anomalies' sources but amplifies noise.

4. Results and Discussions

In order to obtain the total magnetic anomalies, the earth's magnetic field data of our study area were corrected using the 2015 International Geomagnetic Reference Field (IGRF) data implemented in the software Oasis montaj 8.4 (**Figure 4**).

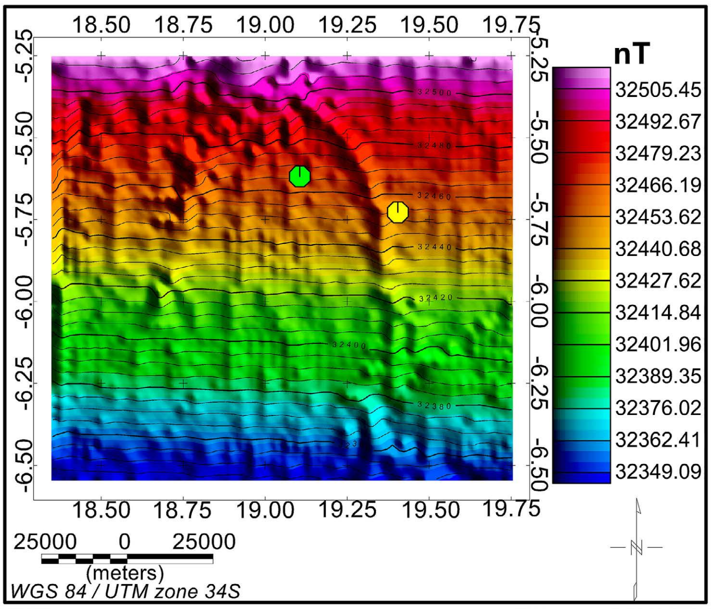

Figure 4. Earth's magnetic field of our study area according to the 2015 International Geomagnetic Reference Field (IGRF) data. Kakobola in green circle and Gungu in yellow circle.

The total magnetic anomalies of our study area obtained after correction are represented in **Figure 5**.

Our study area is characterized by negative values of magnetic anomalies according to the data set. The northeast of the region and the entire central part are generally characterized by high values of the magnetic anomalies. Low values of magnetic anomalies are observed in the North-West and South-East of our study area. These low values vary between −84.5 nT and −87.5 nT while the high values range from −82.7 nT to greater than −81.0 nT. Mean values ranging from −82.8 nT to −84.0 nT are also observed in the region. Both Kakobola and Gungu are located in an area of high magnetic anomalies (**Figure 5**).

Upward continuation filter at elevation of 500 m applied to total magnetic anomalies of our area study leads to high regional magnetic anomalies at the north-eastern county and low regional magnetic anomalies at the western and the eastern-southern parts of our study area (**Figure 6**).

The RTE magnetic anomalies are represented in **Figure 7**.

Low and medium SD values, varying between 0.00 and 0.44 nT, are observed at the north-eastern of our study area and in the Center and the south-western part of the same area (**Figure 8**). These values can be attributed to a little variation in data and thus homogeneity in subsurface structures. High SD values of magnetic anomalies, perceptible in the North-West, the South-East of study area and ranging between 0.44 and 0.96 nT, indicate large variation in data and probably different buried structures of different densities or magnetic susceptibilities. A minutious examination of SD map (**Figure 8**) reveals that high SD values are located in the bed and in the vicinity of major rivers of the study area. These rivers' beds could contain minerals with a high iron oxide content.

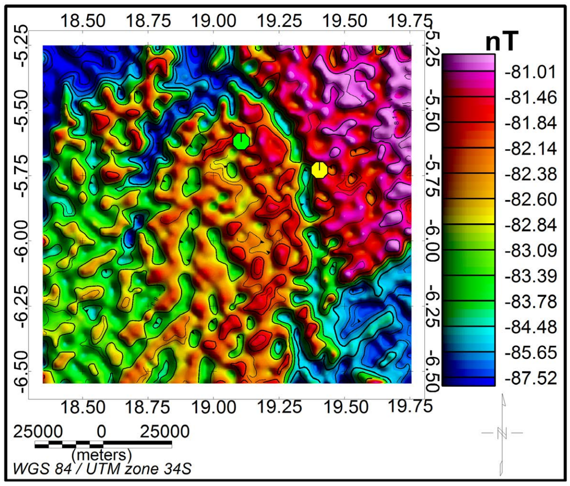

Figure 5. Total magnetic anomalies of our region obtained after correction. Kakobola in green circle and Gungu in yellow circle.

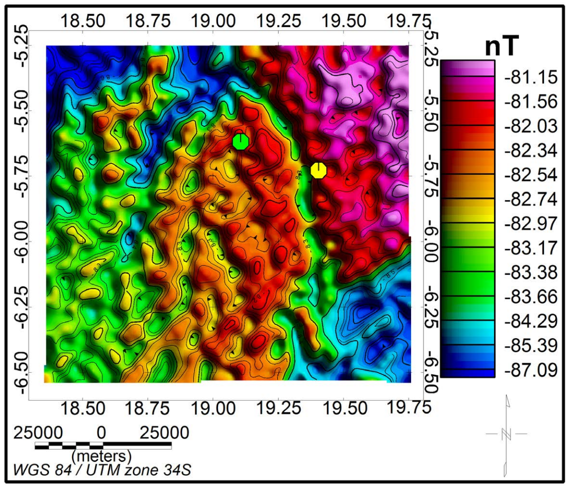

(a)

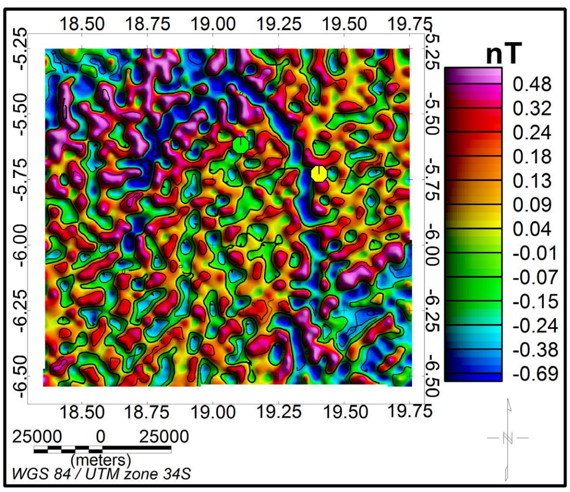

(b)

Figure 6. (a) Regional magnetic anomalies of our study area. (b) Residual magnetic anomalies of our study area. Kakobola in green circle and Gungu in yellow circle.

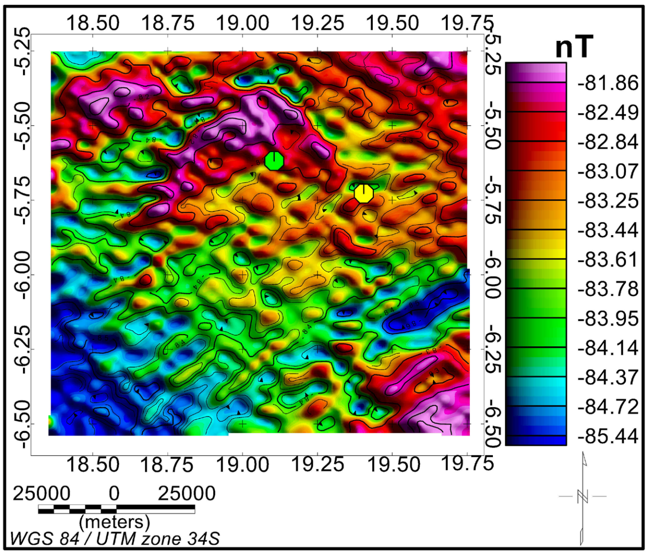

Figure 7. The RTE magnetic anomalies of the study area. Kakobola in green circle and Gungu in yellow circle.

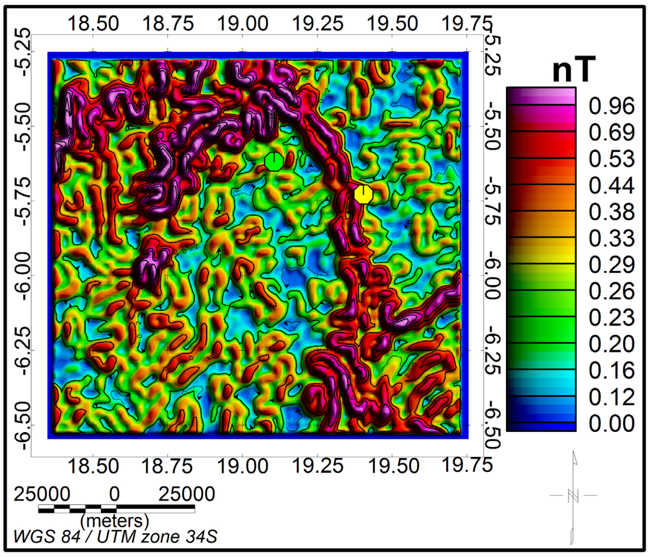

Figure 8. SD map of total magnetic anomalies of the study area. Kakobola in green circle and Gungu in yellow circle.

Our study area is characterized by HGM values ranging from less than 3.03 nT/m to greater than 53.13 nT/m. The high HGM values are principally observed in the North-West, the South-East (**Figure 9**) and could be attributed to shallow sources of magnetic rocks located in the bed and in the neighborhood of major rivers of the region. Mwanamoki et al. (2015) observed a high content of iron in sediment cores sampled from Congo River and Ma Vallée Lake as attested by Table 2 in their paper. This may explain why some HGM values observed in the region are located in the bed of the major rivers of the study area. Low HGM values are observed throughout the central part and in the North-East in the study area; these low HGM values could delineate, in the study

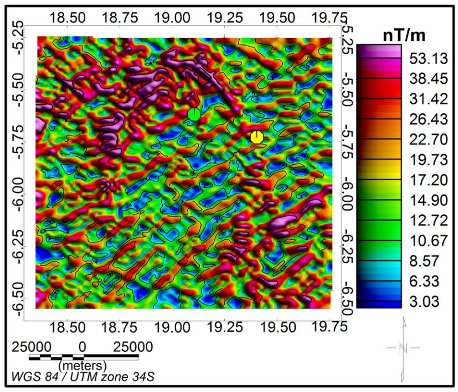

(a)

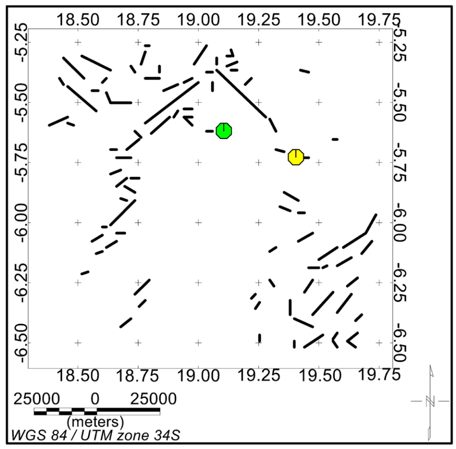

(b)

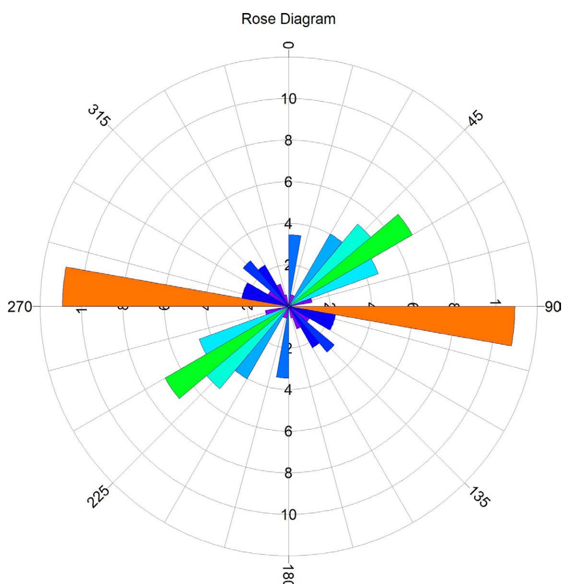

(c)

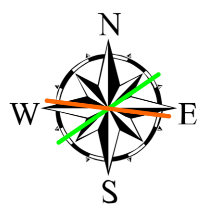

(d)

Figure 9. (a) Horizontal gradient magnitude of RTE magnetic anomalies of our study area. (b) Lineaments derived from HGM of RTE magnetic anomalies of our study area. (c) Rose diagram of lineaments derived from HGM of RTE magnetic anomalies of our study area. (d) Wind rose of lineaments derived from HGM of RTE magnetic anomalies of our study area. Kakobola in green circle and Gungu in yellow circle.

area, shallow cavities, diamagnetic sources and rocks with a fairly low iron oxide content. Gungu is located in a site where HGM values are ranging from 6.33 nT/m to 38.45 nT/m while Kakobola is located in the HGM range from 14.90 nT/m to 19.73 nT/m. Kakobola and Gungu are both crossed by faults as shown in **Figure 9**. The faults and/or fractures in our study area have two preferential directions: W-E, being the most abundant in the region, and NE-SW.

Our study area is characterized by AS ranging from less than 11.70 nT/m to greater than 136.10 nT/m (**Figure 10**). The high AS values are observed in the NW, the SE and isolated lines in the central part and in the NE of our study area. The high AS values can also be attributed to shallow sources of magnetic anomalies located in the bed and in the neighborhood of major rivers of the region. Low AS values are observed throughout the central part and in the NE of the study area; they could delineate cavities, diamagnetic sources or low magnetic sources near the surface of the study area. Gungu is located in a site where AS values are ranging from 79.48 nT/m to 98.68 nT/m while Kakobola is located in the AS range from 57.71 nT/m to 66.79 nT/m. The faults and/or fractures derived from AS map of the total magnetic anomalies of our study area have two preferential directions: W-E and N-S.

The positive TA values varying between 8.89 and 71.66 deg are observed over magnetic sources in our study area while the negative TA values, restricted in the range −78.05 to 0 deg, characterize non-magnetic sources or too deeper and/or low magnetic anomaly sources (**Figure 11**). Magnetic sources present in this study area and delineated by the TA filter are almost linear and connected to each other, as shown in **Figure 11**. As TA filter produces secondary edges around the true edge (Prasad et al., 2022), TA does not delineate bodies correctly. Thus, the magnetic source boundaries revealed par TA in our study area should be taken with care.

The northern part is seriously very fractured. The lineaments show three preferential directions: NW-SE, EEN-WWS and W-E.

Kakobola would be located at the edges of a fault and/or fracture with an inclination of −1.36 radian and in SE-NE direction (**Figure 11(a)**). The city of Gungu would be located between a fault and/or fracture showing on the one hand an inclination of 1.24 radian in its southern part and on the other hand an inclination of −1.36 radian in its northern part. The faults and/or fractures in our study area show two preferential directions: NE-SW and W-E.

Low TM values ranging between 8.93 and 44.86 deg delineate magnetic bodies present in our study area. Nevertheless, secondary produced around true edges blur the map (Prasad et al., 2022) and thus, identification of borders is difficult as shown in **Figure 12**. Magnetic sources are almost linear. Gungu and Kakobola cities are both located between fractures and/or lithological contacts whose dip values vary between 65.39˚ and 78.68˚ (**Figure 12**). The fractures and/or lithological contacts are principally oriented in the directions ENE-WSW and W-E.

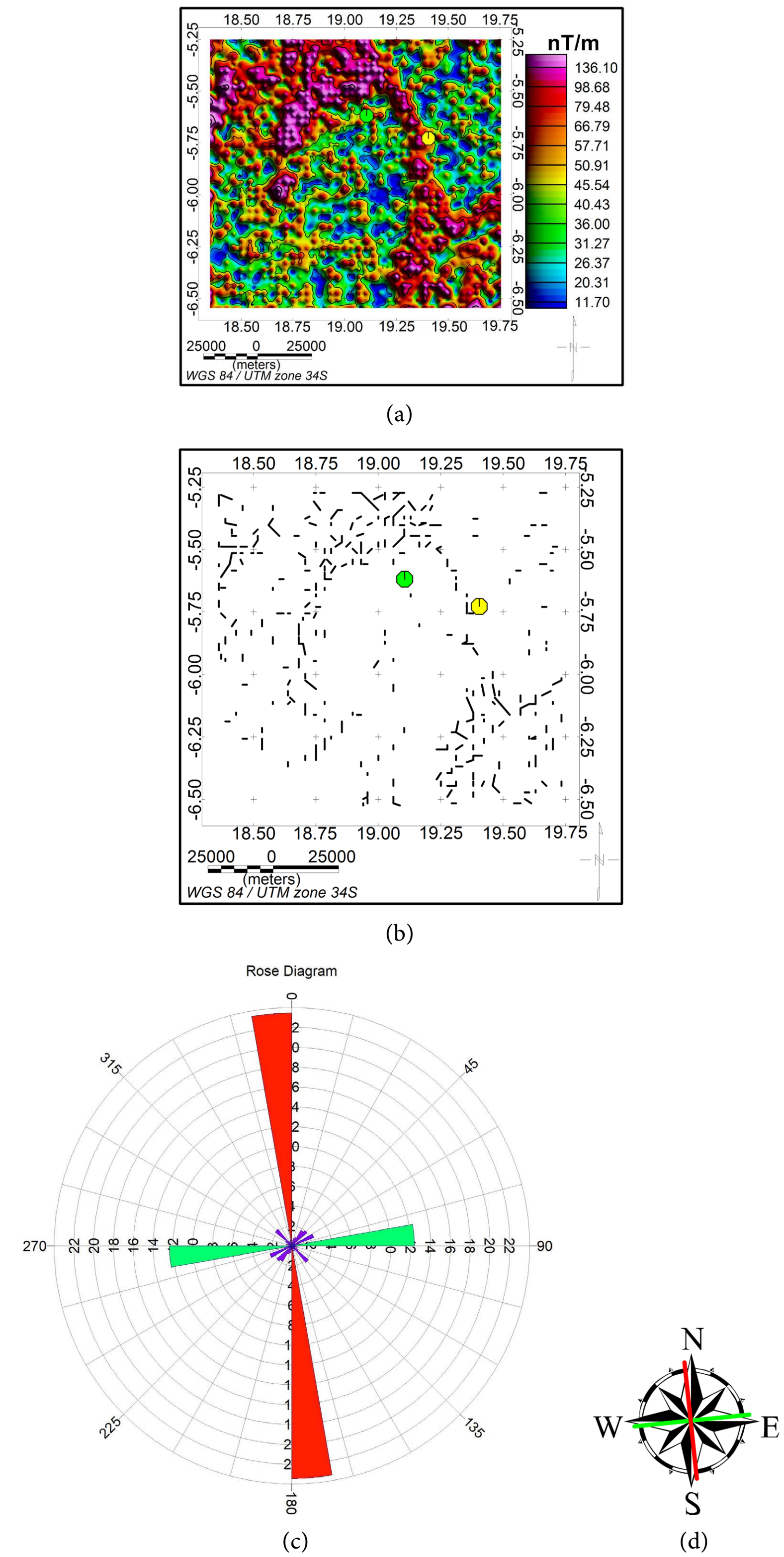

Figure 10. (a) AS map of the total magnetic anomalies of our study area. (b) Lineaments derived from AS map of the total magnetic anomalies of our study area. (c) Rose diagram lineaments derived from AS map of the total magnetic anomalies of our study area. (d) Wind rose of lineaments derived from AS map of the total magnetic anomalies of our study area. Kakobola in green circle and Gungu in yellow circle.

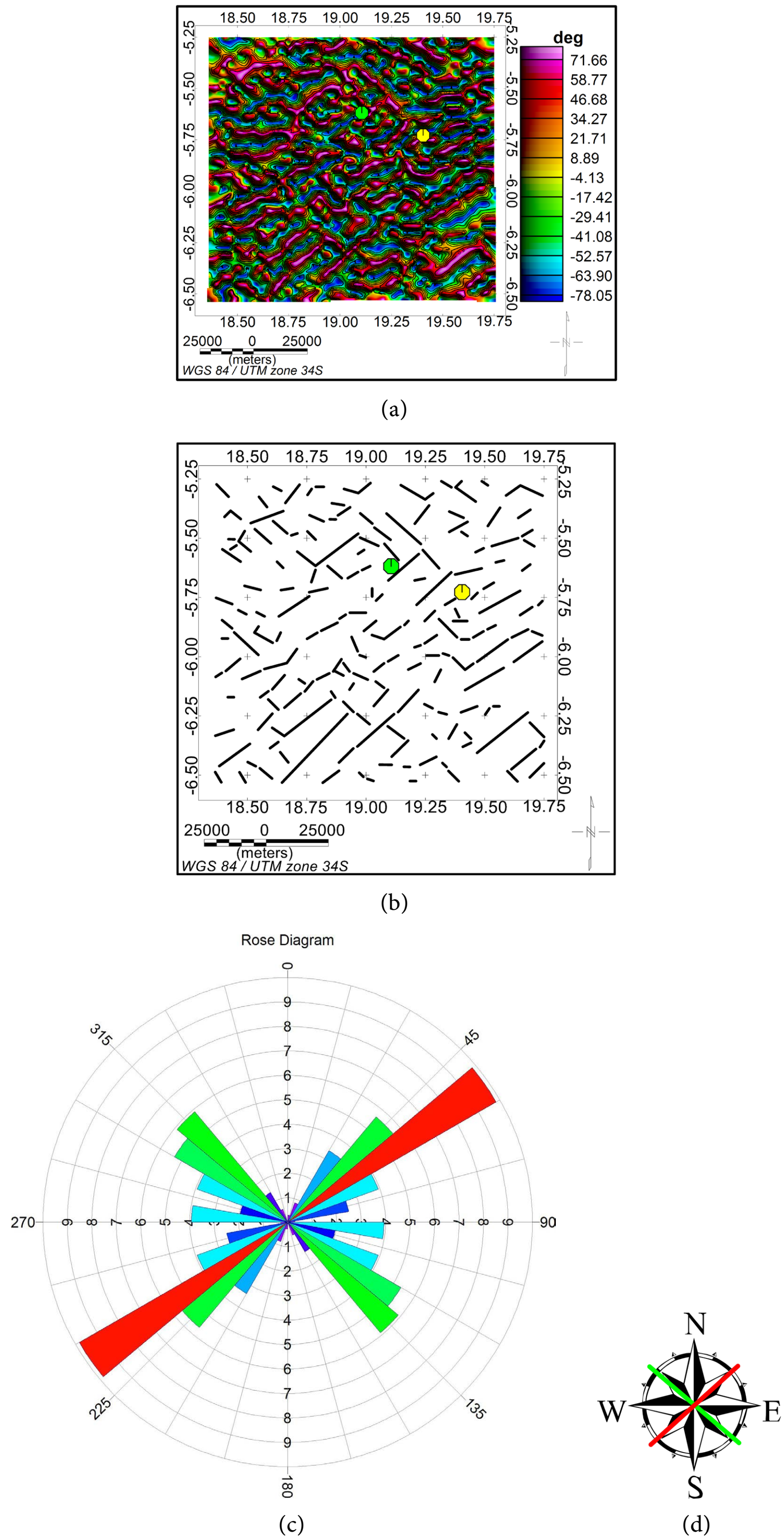

Figure 11. (a) TA map of RTE magnetic anomalies of our study area. (b) Lineaments from TA map of RTE magnetic anomalies of our study area. (c) Rose diagram of lineaments from TA map of RTE magnetic anomalies of our study area. (d) Wind rose of lineaments from TA map of RTE magnetic anomalies of our study area. Kakobola in green circle and Gungu in yellow circle.

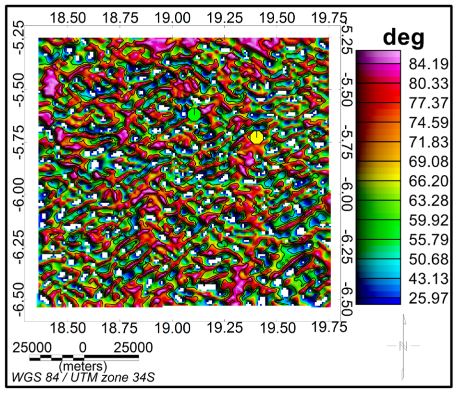

(a)

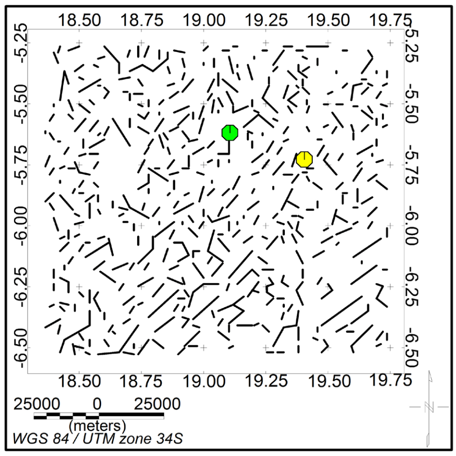

(b)

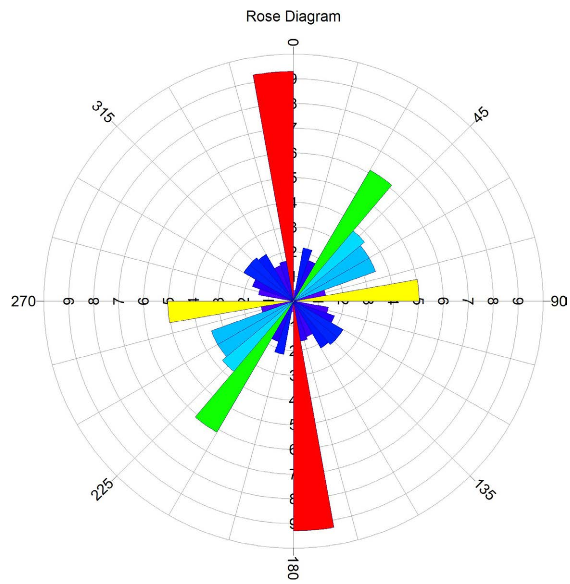

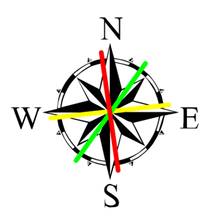

(c) (d)

Figure 12. (a) TM map of RTE magnetic anomalies of our study area. (b) Lineaments from TM map of RTE magnetic anomalies of our study area. (c) Rose diagram of lineaments from TM map of RTE magnetic anomalies of our study area. (d) Wind rose of lineaments from TM map of RTE magnetic anomalies of our study area. Kakobola in green circle and Gungu in yellow circle.

High HGTA values, ranging between 0.03 and 0.07 deg/m, delineate shallow magnetic structures in our study area while low HGTA values are attributed to non-magnetic sources, too low magnetic anomalies' sources or too deeper sources present in the study area (**Figure 13**). However, Arisoy and Dikmen (2013) affirm that results of HGTA filter for deeper bodies are not effective and noise can be amplified if noise is present in data. Magnetic sources identified by HGTA filter in our study area are almost linear and connected. Thus, identification of edges in our study area by this filter can be laborious.

High ETILT values, varying between 0.10 and 0.74 deg, delineate structures of high magnetic anomalies in our study area while low ETILT values can be linked to cavities, to deep magnetic structures or to low magnetized structures. Low dip values revealed by the ETILT filter applied to RTE magnetic anomalies in our study area are linked to tabular structures. This is in agreement with the observations of Mbata Muliwavyo et al. (2023). Kakobola and Gungu are located on sites characterized by low dip values as shown in **Figure 14**. Lineaments derived from ETILT map are principally oriented in the directions: NE-SW, ENE-SWS, NW-SE and W-E (**Figure 14(c)**).

Maximum ETHDR values, varying between 0.11 deg/m and 0.23 deg/m, delineate magnetic sources in our study area (**Figure 15**). Low ETHDR values between 0.02 and 0.11 deg/m can be attributed to non-magnetic sources, to cavities or to deeper magnetic sources. Sources of magnetic anomalies are connected as shown in **Figure 15**. Care must be taken because noise is amplified by the ETHDR filter (Arisoy & Dikmen, 2013).

Maximum TAHG values in our study value vary between 8.28 and 70.61 deg and highlight borders of magnetic anomalies sources at different depths in our study area (**Figure 16**). Negative TAHG values in our study area can be attributed to too deeper magnetic sources, non-magnetic sources or too low anomalies' sources. Low resolution of edges detected (Prasad et al., 2022) can affect delineation of magnetic bodies in this study area. Low, medium and high dip values of lineaments derived from TAHG map characterize the study area. Some magnetic sources are almost linear and connected as attested in **Figure 16**. Gungu and Kakobola cities are located between fractures and/or lithological contacts whose dip values are high.

Maximum TAAS values in our study value vary between 9.17 and 66.06 deg and highlight borders of magnetic anomalies sources at different depths in our study area (**Figure 17**). Negative TAAS values in our study area can be attributed to too deeper sources of magnetic anomalies, non-magnetic sources or too low anomalies' sources. Low resolution of edges detected (Prasad et al., 2022) can affect delineation of magnetic bodies in this study area. Low, medium and high dip values of lineaments derived from TAAS map may characterize all the study area as attested in **Figure 17**. Gungu and Kakobola cities are both located between fractures and/or lithological contacts whose dip values are high. The preferential directions of lineaments according to TAAS results are W-E, N-S, NW-SE, WNW-ESE and NNE-SSW.

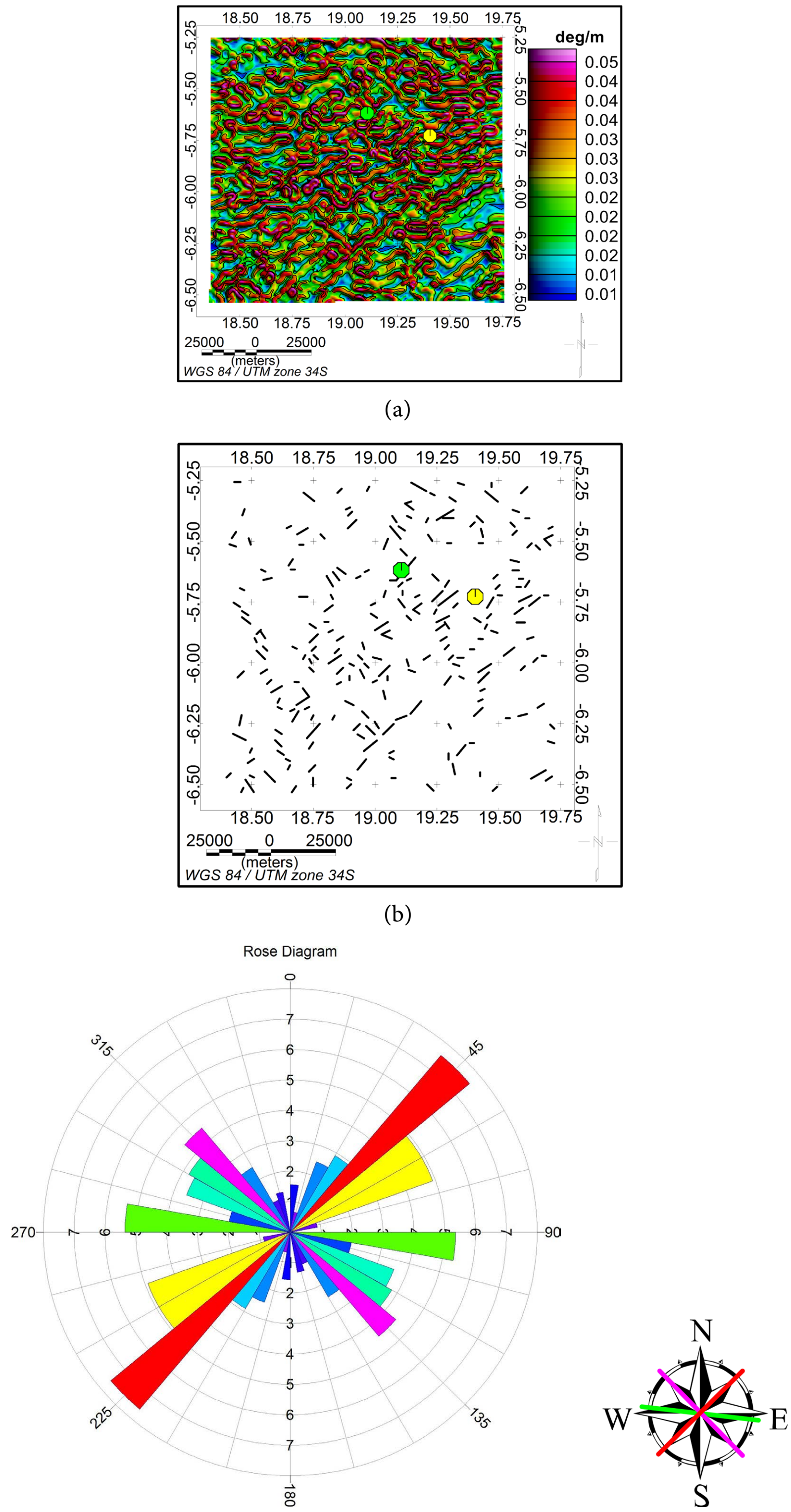

Figure 13. (a) HGTA map of RTE magnetic anomalies of our study area. (b) Lineaments derived from HGTA map of RTE magnetic anomalies of our study area. (c) Rose diagram of lineaments derived from HGTA map of RTE magnetic anomalies of our study area. (d) Wind rose of lineaments derived from HGTA map of RTE magnetic anomalies of our study area. Kakobola in green circle and Gungu in yellow circle.

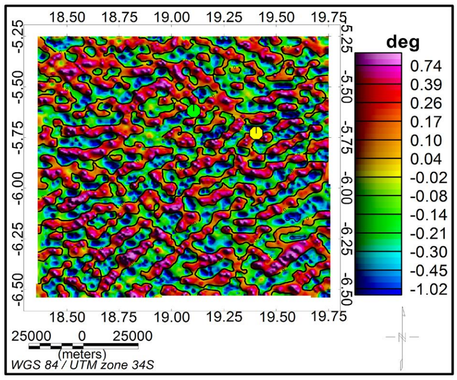

(a)

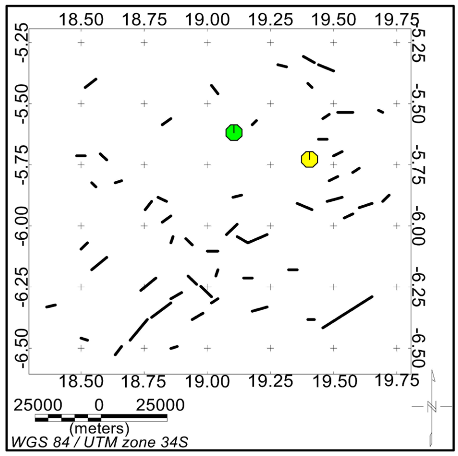

(b)

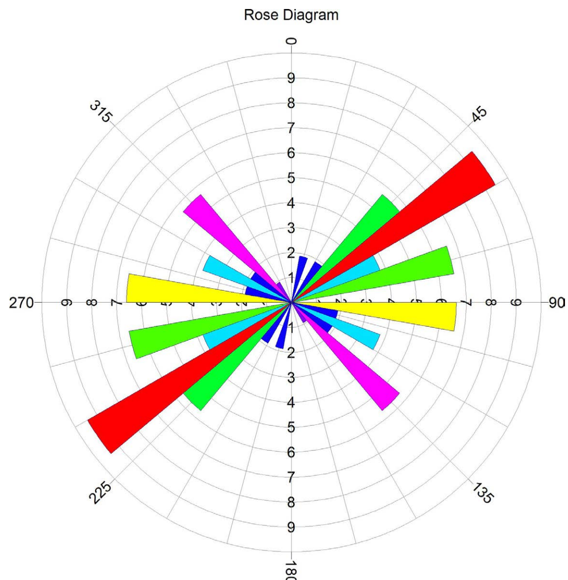

(c)

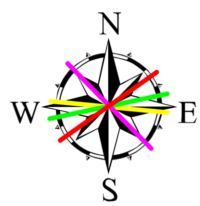

(d)

Figure 14. (a) ETILT map of RTE magnetic anomalies of our study area. (b) Lineaments from ETILT map of RTE magnetic anomalies of our study area. (c) Rose diagram of lineaments from ETILT map of RTE magnetic anomalies of our study area. (d) Wind rose of lineaments from ETILT map of RTE magnetic anomalies of our study area. Kakobola in green circle and Gungu in yellow circle.

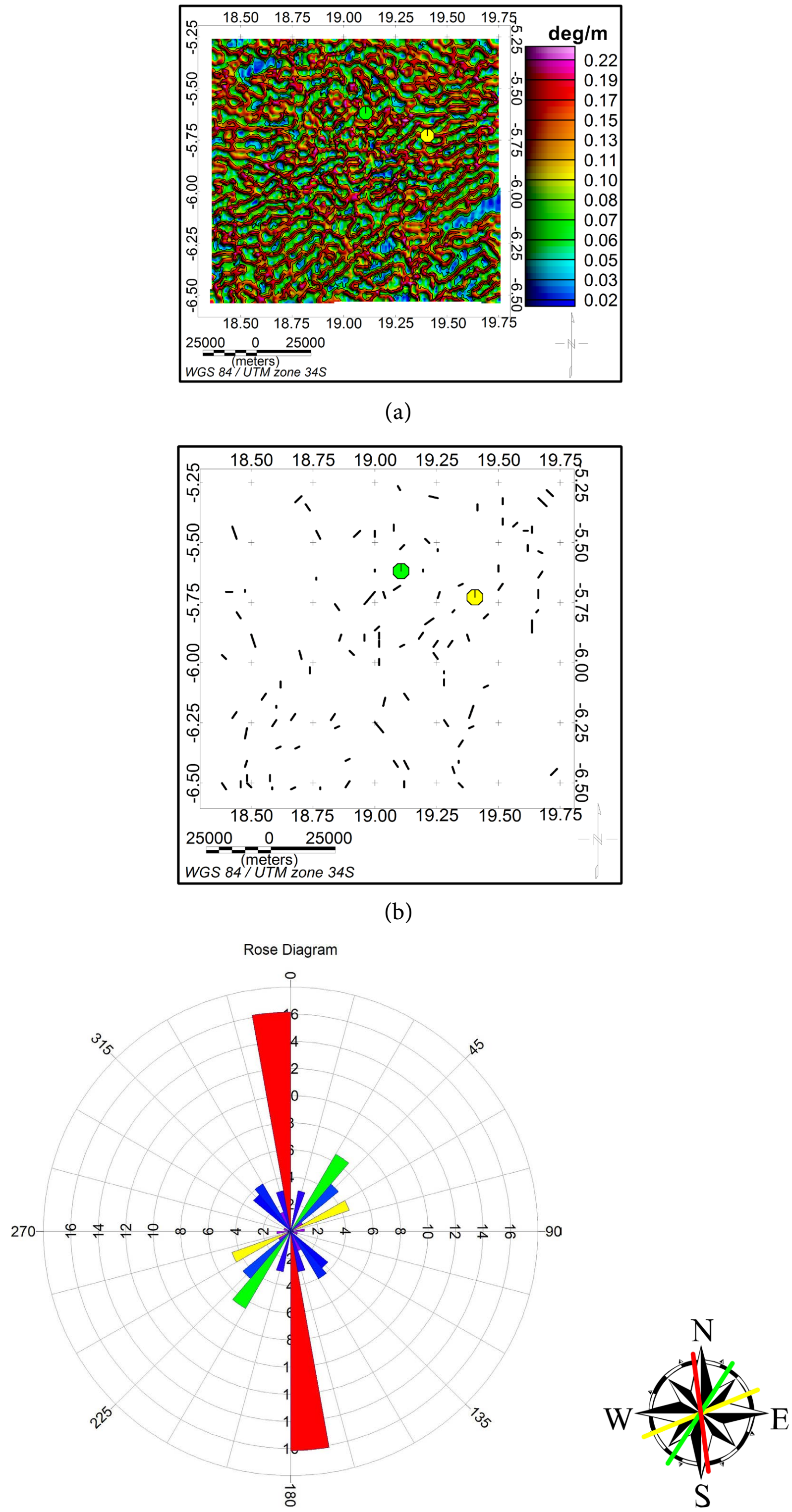

(a) (b) (c) (d)

Figure 15. (a) ETHDR map of RTE magnetic anomalies of our study area. (b) Lineaments from ETHDR map of RTE magnetic anomalies of our study area. (c) Rose diagram of lineaments from ETHDR map of RTE magnetic anomalies of our study area. (d) Wind rose of lineaments from ETHDR map of RTE magnetic anomalies of our study area. Kakobola in green circle and Gungu in yellow circle.

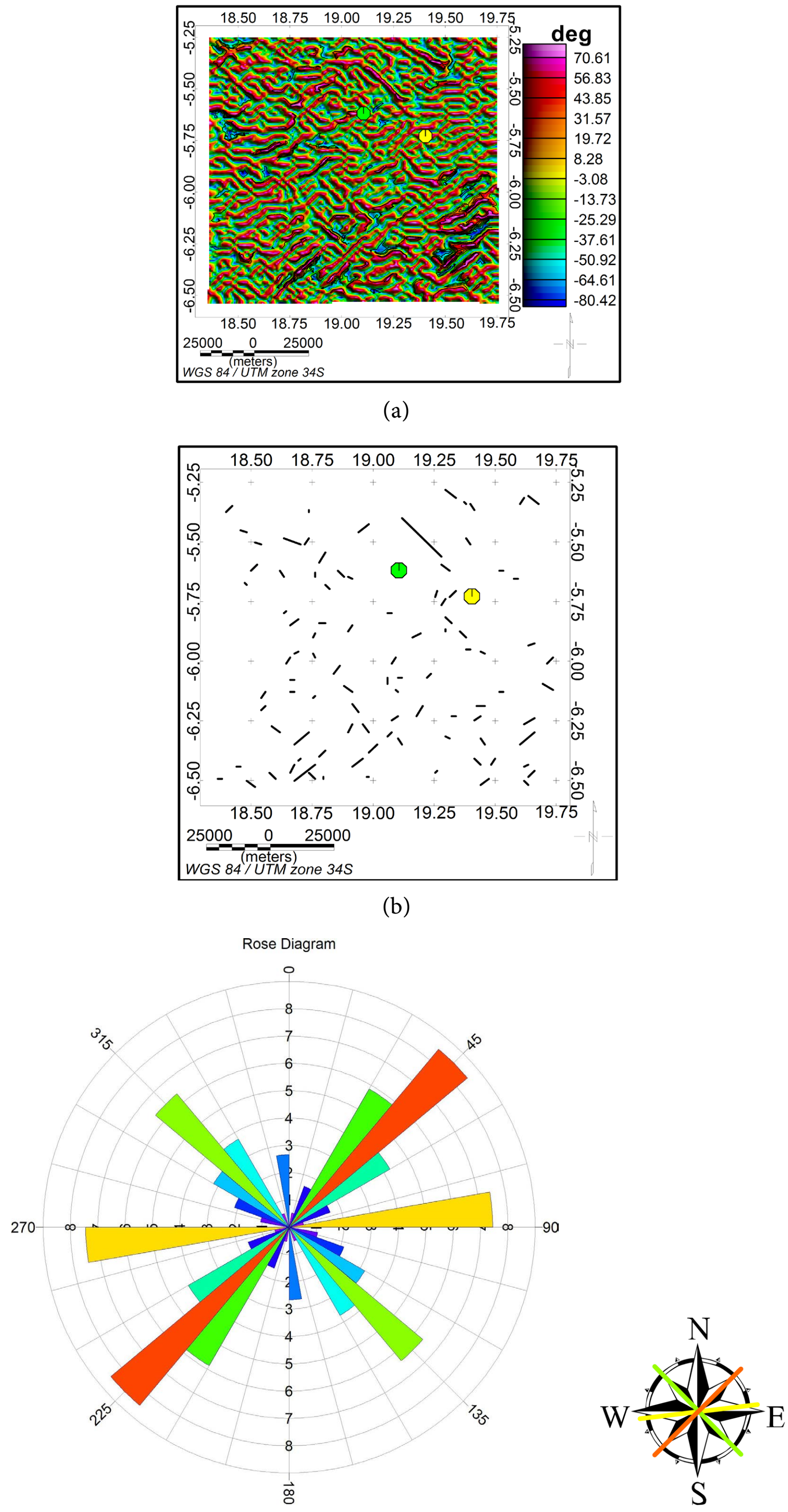

Figure 16. (a) TAHG map of RTE magnetic anomalies of our study area. (b) Lineaments derived from TAHG map of RTE magnetic anomalies of our study area. (c) Rose diagram of lineaments derived from TAHG map of RTE magnetic anomalies of our study area. (d) Wind rose of lineaments derived from TAHG map of RTE magnetic anomalies of our study area. Kakobola in green circle and Gungu in yellow circle.

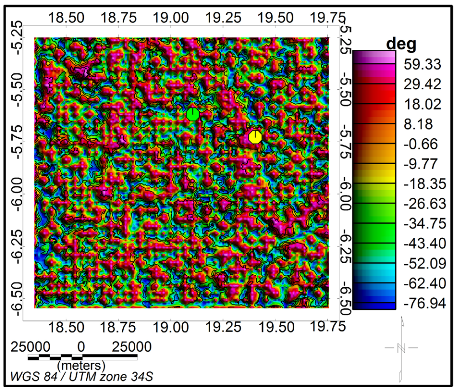

(a)

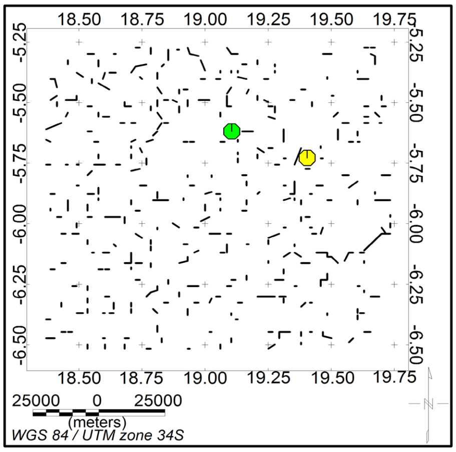

(b)

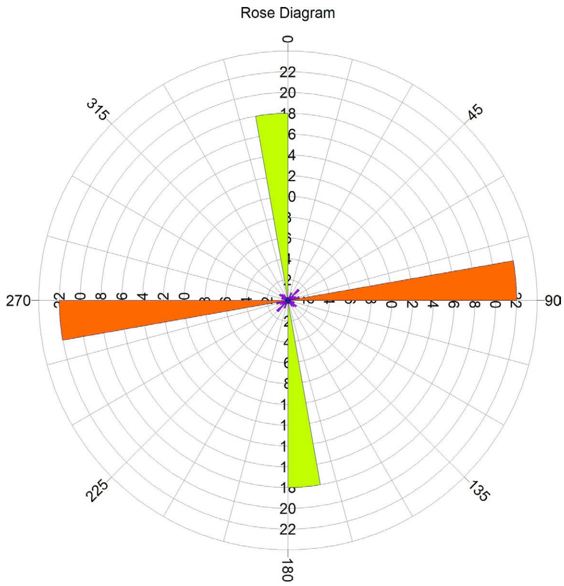

(c)

(d)

Figure 17. (a) TAAS map of total magnetic anomalies of our study area. (b) Lineaments derived from TAAS map of total magnetic anomalies of our study area. (c) Rose diagram of lineaments derived from TAAS map of total magnetic anomalies of our study area. (d) Wind rose of lineaments derived from TAAS map of total magnetic anomalies of our study area. Kakobola in green circle and Gungu in yellow circle.

5. Conclusion

Sources of low magnetic anomalies are located at the South-East and the North-West of the study area while sources of high magnetic anomalies are located at the East and at the West of the Kwilu River. The shallow sources of magnetic anomalies are located in the bed and in the vicinity of the Kwilu River, and in the North-West and the South-East of the study area. The borders of shallow and deep sources of magnetic anomalies present in our study area reveal that the magnetic sources in the study area are almost linear and connected to each other. Several magnetic lineaments identified in this region present several preferential directions but the most predominant directions are NE-SW, NW-SE, W-E and NE-SW. A harmonious development of Kakobola and its surroundings requires taking into account the presence of cavities and fractures or lithological contacts in this region. A structural study of this region, based on high-resolution geomagnetic data, should be carried out in order to correctly locate and delineate the cavities, evaluate their depths and position exactly the fractures and/or the lithological contacts on the site.

Conflicts of Interest

The authors declare no conflicts of interest regarding the publication of this paper.

References

Arisoy, M., & Dikmen, Ü. (2013). Edge Detection of Magnetic Sources Using Enhanced Total Horizontal Derivative of the Tilt Angle. *Bulletin of the Earth Sciences Application and Research Centre of Hacettepe University, 34,* 73-82.

Blakely, R. (1995). *Potential Theory in Gravity and Magnetic Applications* (pp. 311-358). Cambridge University Press. https://doi.org/10.1017/CBO9780511549816.

Cooper, G. R. J. (2014). Reducing the Dependence of the Analytic Signal Amplitude of Aeromagnetic Data on the Source Vector Direction. *Geophysics, 79,* J55-J60. https://doi.org/10.1190/geo2013-0319.1

Cordell, L., & Grauch, V. J. (1982). Mapping Basement Magnetization Zones from Aeromagnetic Data in the San Juan Basin, New Mexico. In *52nd Annual International Meeting* (pp. 246-248). Society of Exploration Geophysicists. https://doi.org/10.1190/1.1826915

De Ploey, J., Lepersonne, J., & Stoops, G. (1968). *Sédimentologie et origine des sables de la série des sables ocre et de la série des grès polymorphes (système du Kalahari) au Congo occidental*. Annales des Sciences Géologiques, Série No. 61, Musée Royal de l'Afrique Centrale, 69-72.

Domzalski, W. (1966). Interpretation of Aeromagnetic in Evaluation of Structural Control of Mineralization. *Geophysical Prospecting, 14,* 273-291. https://doi.org/10.1111/j.1365-2478.1966.tb01761.x

Eldosouky, A. M., Thanh Pham, L., Mohmed, H., & Pradhan, B. (2020). A Comparative Study of THG, AS, TA, Theta, TDX and LTHG Techniques for Improving Source Boundaries Detection of Magnetic Data Using Synthetic Models: A Case Study from G. Um Monqul, North Eastern Desert, Egypt. *Journal of African Earth Sciences, 170,* Article ID:

103940. https://doi.org/10.1016/j.jafrearsci.2020.103940

Elkhateeb, S. O., Eldosouky, A. M., & Aboelabas, S. (2018). Interpretation of Aeromagnetic Data to Delineate Structural Complexity Zones and Porphyry Intrusions at Samr El Qaa Area, North Eastern Desert, Egypt. *International Journal of Novel Research in Civil Structural and Earth Sciences, 5,* 1-9.

Ferreira, F. J. F., de Souza, J., Bongiolo, A. de B. e S., & de Castro, L. G. (2013). Enhancement of the Total Horizontal Gradient of Magnetic Anomalies Using the Tilt Angle. *Geophysics, 78,* J33-J41. https://doi.org/10.1190/geo2011-0441.1

Ghil, M., Allen, M. R., Dettinger, M. D., Ide, K., Kondrashov, D., Mann, M. E. et al. (2002). Advanced Spectral Methods for Climatic Time Series. *Reviews of Geophysics, 40,* 3-1-3-41. https://doi.org/10.1029/2000RG000092

Keating, P., & Sailhac, P. (2004). Use of the Analytic Signal to Identify Magnetic Anomalies Due to Kimberlite Pipes. *Geophysics, 69,* 180-190. https://doi.org/10.1190/1.1649386

Mbata Muliwavyo, A., Musitu Muliwavyo, J., Tshitenge Mbuebue, J.-M., Musitu, L., & Umba-Di-Mbudi, C. N. (2023). Structural Study of the Kakobola Area and Its Surroundings by Detecting the Edges of Gravity Anomaly Sources. *Journal of Geoscience and Environment Protection, 11,* 81-97. https://doi.org/10.4236/gep.2023.117006

Miller, H. G., & Singh, V. (1994). Potential Field Tilt—A New Concept for Location of Potential Field Sources. *Journal of Applied Geophysics, 32,* 213-217. https://doi.org/10.1016/0926-9851(94)90022-1

Mwanamoki, P. M., Devarajan, N., Niane, B., Ngelinkoto, P., Thevenon, F., Nlandu, J. W. et al. (2015). Trace Metal Distributions in the Sediments from River-Reservoir Systems: Case of the Congo River and Lake Ma Vallée, Kinshasa (Democratic Republic of Congo). *Environmental Science and Pollution Research, 22,* 586-597. https://doi.org/10.1007/s11356-014-3381-y

Nabighian, M. N. (1972). The Analytic Signal of Two-Dimensional Magnetic Bodies with Polygonal Cross-Section: Its Properties and Use for Automated Anomaly Interpretation. *Geophysics, 37,* 507-517. https://doi.org/10.1190/1.1440276

Nasuti, Y., & Nasuti, A. (2018). NTilt as an Improved Enhanced Tilt Derivative Filter for Edge Detection of Potential Field Anomalies. *Geophysical Journal International, 214,* 36-45. https://doi.org/10.1093/gji/ggy117

Nasuti, Y., Nasuti, A., & Moghadas, D. (2018). STDR: A Novel Approach for Enhancing and Edge Detection of Potential Field Data. *Pure and Applied Geophysics, 176,* 827-841. https://doi.org/10.1007/s00024-018-2016-5

Ndala, T. I., Kalanga, K. B., Musitu, M. J., Mpiana, K. C., Kanda, N. V., & N'Zau Umba-di-Mbudi, C. (2022). Caractérisations sédimentologique et pale environnementale du site de l'aménagement hydroélectrique deKakobola et ses environs (Province du Kwilu/RD Congo). *Geo-Eco-Trop, 46,* 315-328.

Ndala, T. I., Musitu, M. J., Kalanga, K. B., & N'Zau Umba-di-Mbudi, C. (2023). Caractérisation des grès Ceno-Mesozoiques du site d'aménagement hydroélectrique de Kakobola et ses environs par diffraction et fluorescence X (Province du Kwilu/RD Congo). *Geo-Eco-Trop, 2,* 329-342.

Pham, L. T. (2020). A Comparative Study on Different Filters for Enhancing Potential Field Source Boundaries: Synthetic Examples and a Case Study from the Song Hong Trough (Vietnam). *Arabian Journal of Geosciences, 13,* Article No. 723. https://doi.org/10.1007/s12517-020-05737-5

Pham, L. T., Eldosouky, A. M., Oksum, E., & Saada, S. A. (2022). A New High Resolution

Filter for Source Edge Detection of Potential Field Data. *Geocarto International, 37,* 3051-3068. https://doi.org/10.1080/10106049.2020.1849414

Pham, L. T., Oksum, E., Do, T. D., Nguyen, D. V., & Eldosouky, A. M. (2021a). On the Performance of Phase-Based Filters for Enhancing Lateral Boundaries of Magnetic and Gravity Sources: A Case Study of the Seattle Uplift. *Arabian Journal of Geosciences, 14,* Article No. 129. https://doi.org/10.1007/s12517-021-06511-x

Pham, L. T., Vu, M. D., & Le, S. T. (2021b). Performance Evaluation of Amplitude- and Phase-Based Methods for Estimating Edges of Potential Field Sources. *Iranian Journal of Science and Technology, Transaction A: Science, 45,* 1327-1339. https://doi.org/10.1007/s40995-021-01122-3

Prasad, K. N. D., Pham, L. T., Singh, A. P., Eldosouky, A. M., Abdelrahman, K., Fnais, M. S., & Gómez-Ortiz, D. (2022). A Novel Enhanced Total Gradient (ETG) for Interpretation of Magnetic Data. *Minerals, 12,* Article 1468. https://doi.org/10.3390/min12111468

Roest, W. R. J., Verhoef, J., & Pilkington, M. (1992). Magnetic Interpretation Using the 3-D Analytic Signal. *Geophysics, 57,* 116-125. https://doi.org/10.1190/1.1443174

Salem, A., Simon, W., Fairhead, J. D., Ravat, D., & Smith, R. (2007). Tilt-Depth Method: A Simple Depth Estimation Methodusing First-Order Magnetic Derivatives. *The Leading Edge, 26,* 1502-1505. https://doi.org/10.1190/1.2821934

Souga, K. V., Ndougsa, M. T., Meying, A., Ngoh, J., & Ngoa, E. S. (2020). Structural Features Derived from a Multiscale Analysis and 2.75D Modelling of Aeromagnetic Data over the Pitoa-Figuil Area (Northern Cameroon). *EGU (European Geosciences Union),* 1-18.

Tshiwisa, I. N., Mayena, T. K., Osomba, D. W., Muliwavyo, A. M., Kabuya, B. K., Muliwavyo, J. M., & Umba-Di-Mbudi, C. N. (2023). On the Origin of the Cavities Present in the Sandstone Formations of the Hydroelectric Development Site of Kakobola and Its Surroundings (Kwilu Province/DRC). *Journal of Geoscience and Environment Protection, 11,* 170-191. https://doi.org/10.4236/gep.2023.114010

Verduzco, B., Fairhead, J. D., Green, C. M., & MacKenzie, C. (2004). New Insights into Magnetic Derivatives for Structural Mapping. *The Leading Edge, 23,* 116-119. https://doi.org/10.1190/1.1651454

Wijns, C., Perez, C., & Kowalczyk, P. (2005). Theta Map: Edge Detection in Magnetic Data. *Geophysics, 70,* 39-43. https://doi.org/10.1190/1.1988184